HHS Public Access

Author manuscript

Adv Mater. Author manuscript; available in PMC 2024 April 01.

Published in final edited form as:

Adv Mater. 2023 April ; 35(15): e2207255. doi:10.1002/adma.202207255.

Engineered Living Intestinal Muscle Patch Produces Macroscopic Contractions that can Mix and Break down Artificial Intestinal Contents

Qianqian Wang[*,[+]],
Division of Pediatric Surgery, Departments of Surgery and Bioengineering, Stanford University School of Medicine, Stanford, California 94305, USA

Jiafang Wang,
Division of Pediatric Gastroenterology and Nutrition, Department of Pediatrics, David Geffen School of Medicine at UCLA, Los Angeles, California 90095, USA

Elmira Tokhtaeva,
Division of Pediatric Gastroenterology and Nutrition, Department of Pediatrics, David Geffen School of Medicine at UCLA, Los Angeles, California 90095, USA

Zhen Li,
Division of Pediatric Surgery, Departments of Surgery and Bioengineering, Stanford University School of Medicine, Stanford, California 94305, USA

Martín G. Martín,
Division of Pediatric Gastroenterology and Nutrition, Department of Pediatrics, David Geffen School of Medicine at UCLA, Los Angeles, California 90095, USA

Xuefeng B. Ling,
Division of Pediatric Surgery, Departments of Surgery and Bioengineering, Stanford University School of Medicine, Stanford, California 94305, USA

James C.Y. Dunn[*]
Division of Pediatric Surgery, Departments of Surgery and Bioengineering, Stanford University School of Medicine, Stanford, California 94305, USA

Abstract

The intestinal muscle layers execute various gut wall movements to achieve controlled propulsion and mixing of intestinal content. Engineering intestinal muscle layers with complex contractile function is critical for developing bioartificial intestinal tissue to treat patients with short bowel syndrome. Here we report the first demonstration of a living intestinal muscle patch capable

[*]Corresponding author. jdunn2@stanford.edu; cassieqq@stanford.edu.
[+]Present address: Institute for Stem Cell Biology and Regenerative Medicine, Stanford University School of Medicine, Stanford, California 94305, USA

Conflict of interest
The authors declare no conflict of interest.

Supporting Information
Supporting Information is available from the Wiley Online Library or from the author.

of generating three distinct motility patterns and displaying multiple digesta manipulations. Assessment of cell contractility, cellular morphology, and transcriptome profile reveals that successful generation of the contracting intestinal muscle patch relies on both biological factors in a serum-free medium and environmental cues from an elastic electrospun gelatin scaffold. By comparing gene-expression patterns among samples, we show that biological factors from the medium strongly affect ion transport activities, while the scaffold unexpectedly regulates cell-cell communication. Analysis of the ligand-receptor interactome identifies the scaffold-driven changes in intercellular communication, and 78% of the upregulated ligand-receptor interactions are involved in the development and function of enteric neurons. Our discoveries highlight the importance of combining biomolecular and biomaterial approaches for tissue engineering. The living intestinal muscle patch represents a pivotal advancement for building functional replacement intestinal tissue. It offers a more physiological model for studying GI motility and for preclinical drug discovery.

Graphical Abstract

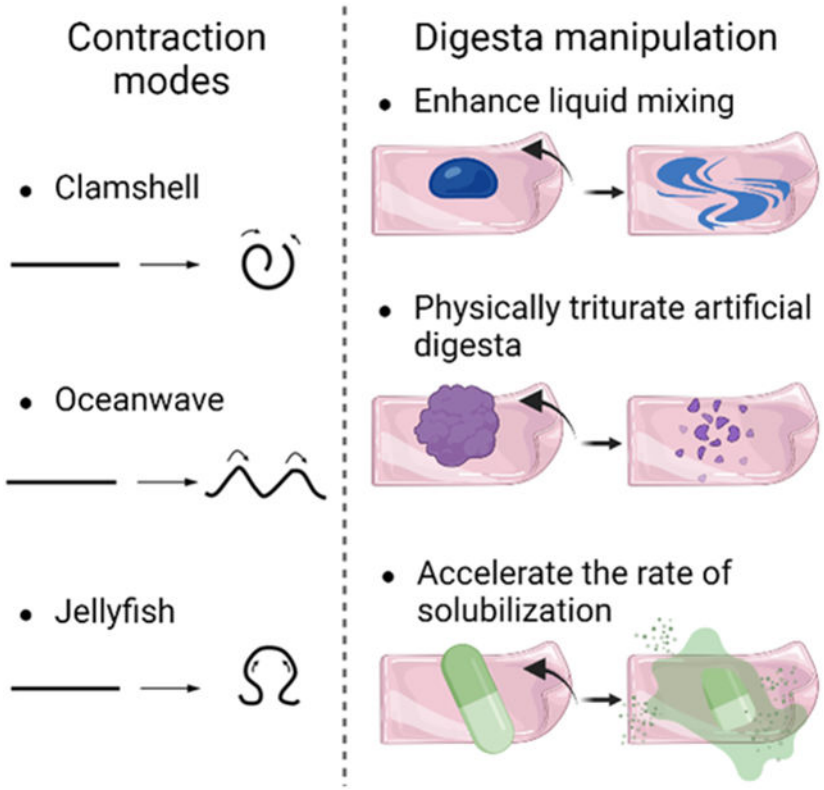

An engineered intestinal muscle patch is created for the first time in vitro to generate three distinct contraction modes. It shows record strength of contractility, strong enough to mix and physically triturate viscoelastic gels that mimic mechanical properties of the intestinal digesta. Generating such muscle patches depends on both biochemical signals from the medium and environmental cues from a bioscaffold.

Keywords

Intestinal smooth muscle regeneration; Intestinal tissue engineering; Living building blocks

1. Introduction

Short bowel syndrome (SBS) is a life-threatening and devastating condition when a massive portion of the bowel length is lost, and the remaining intestine no longer absorbs enough nutrients to sustain life.[1-3] SBS represents the leading cause of intestinal failure.[1,4,5] With no restorative solution available, patients with SBS are mainly managed through prolonged intravenous parenteral nutrition, a treatment associated with poor quality of life, high financial burden, frequent hospitalization, and significant risk of severe complications.[1-6] Despite decades of efforts to optimize the management of SBS, its mortality remains high (up to 30 to 50%).[1,3,7] The striking incidence of death among SBS patients has motivated the search for novel therapies to treat or even cure SBS. Intestinal tissue engineering offers an alternative therapeutic solution for SBS by creating functional neo-intestine. Current advances in intestinal tissue engineering primarily focus on reconstructing the intestinal epithelial layer; however, few have aimed at intestinal muscle regeneration.[6] The intestinal smooth muscle layers subserve multiple important functions,[8-14] among which the best-known function of the intestinal muscle is to generate gut motility for controlled mixing and propulsion of the intestinal contents. The movement of the gut wall physically breaks down food, mixes the food with the digestive secretions, delivers the nutrients toward the absorptive surface, and transports intestinal contents along the tract. Regenerating intestinal smooth muscle layers with appropriate motility functions is crucial for developing a functional artificial intestine.

Even as early as 16 weeks of gestational age, gut motility is detected in human fetuses.[15] Coordinated contractions and relaxations of the circular and longitudinal smooth muscle layers give rise to a rich repertoire of motor patterns, which vary with dietary status, and dynamically change between interdigestive and postprandial states.[14,16] Such various motor patterns are achieved by a multitude of cooperating mechanisms involving different players within the muscle layers, including smooth muscle cells (SMCs), the pacemaker, interstitial cells of Cajal (ICCs), PDGFRα$^+$ cells, and the enteric neurons.[14,17] Each of them forms its delicate cellular network, which intertwines and communicates with the networks of the other players throughout the whole intestine. Contractions of the gut wall require a synchronized movement of thousands of SMCs. To facilitate this highly coordinated activity, SMCs form electrical and mechanical junctions with each other.[14] They are also electrically coupled to their neighboring ICCs and PDGFRα$^+$ cells, creating an electrical syncytium.[14] ICCs within the syncytium generate rhythmic slow waves that simultaneously activate numerous SMCs to force them to contract at the same pace.[18-20] Even the most seemingly simple motility pattern results from dedicated spatial and temporal control of muscle contractions by the enteric nervous system (ENS). For example, propelling the digesta down in the intestine requires SMCs to contract at the site of the digesta but relax in front of it.[21-24] When the digesta enters the intestine, sensory cells first detect the mechanical distortion and the chemical stimuli exerted by the digesta.[25-27] Then, the neural

network relays the transduced signals to the motor neurons, which, in turn, stimulate the organized muscle contraction/relaxation at the designated sites.[14,25,28] Other influencers, such as hormones, immune mediators, intestinal microbiota, and signals from the central nervous system, all participate in fine-tuning the motility patterns for specialized needs.[14,16,17,25,29,30]

Efforts are being invested in regenerating these highly complex functional intestinal muscles. Various engineering strategies have regenerated smooth muscle that shows non-spontaneous contraction.[31-35] Several other pieces of research show that primary intestinal organoids,[36,37] primary cells isolated from the intestinal muscle layers (IMCs),[38,39] or primary intestinal muscle strips[40] can exert spontaneous (in some cases, rhythmic[38,40]) contractions but only for no more than 14 days during in vitro culture. Contractile activity of IMCs can be extended to over ten weeks in vitro when they are co-cultured with feeder cells.[41] Short-term spontaneous contraction can also be achieved in the gut-like structure derived from embryonic stem cells,[42,43] embryonic intestinal progenitor cells,[44] or induced pluripotent stem cells (PSCs)[45] in vitro. For PSC-derived human intestinal organoids (HIOs),[46-48] ICC-dependent spontaneous contractions are observed after HIOs have been transplanted in mice for 6-12 weeks.[49-52] Incorporating uniaxial strain by an intestinal lengthening device enhances spontaneous contractions to a higher amplitude and duration.[52] HIOs exhibit neuron-mediated contractions when combined with PSC-derived neural crest cells or pre-migratory neural crest stem cells.[49-51]

Despite these advances, much work remains to be done before therapeutic avenues can open. Intestinal muscle executes a large variety of motor patterns to mix and break down the intestinal contents. None of the currently available, engineered intestinal smooth muscles can generate multiple types of motor patterns, nor do they display contractions proven to be capable of mixing the enteric content. To engineer intestinal muscle with such strong and diverse modes of contractions, IMCs are the most clinically relevant and readily available cell source. IMCs contain all the critical cell types required for generating gut motility. However, progress in IMC-based intestinal muscle tissue engineering is surprisingly slow, mainly because (*i*) conventional serum-containing culture medium (proliferation medium, P medium) cannot support most of the cell types, and (*ii*) SMCs quickly lose their contractile phenotype in those conditions.[6,14,53] To overcome these problems, our group has developed a serum-free culture medium—the ‘muscularis medium’ (M medium)—that can maintain the maturity and function of SMCs, ICCs, and enteric neurons altogether over a prolonged period in vitro.[53] IMCs in the M medium exhibit ICC- and neuron-dependent spontaneous contractions, which can last for over eight weeks.[53] However, in 2D culture, cells are confined by the stiff substrate of the well plate, and contractions are restricted to locally active cell clusters, which ultimately limits the application of such culture. In the native tissue, IMCs form cellular networks within an extracellular matrix with appropriate mechanical properties to facilitate quick mechanical/electrical transduction. We sought to incorporate a 3D scaffold designed to elicit tissue-matched properties to further promote formation of cell networks and generation of coordinated cell contraction.

In this study, we fabricate an electrospun orthogonal bi-layered scaffold with aligned fibers to mimic the natural geometry of the intestinal muscle layers. More importantly,

we note that previously frequently used material, PCL, dissipates contractile muscle force by deformation and cannot adequately support muscle contractile function. Instead, we apply gelatin, an elastic material, to fabricate such bi-layered scaffolds to better accommodate the cyclic deformation of the muscle. The stiffness of the gelatin scaffold replicates that of the native tissue. The integrated effect of the M medium and the gelatin scaffold results in generation of a living intestinal muscle patch with coordinated macroscopic contractions that can be easily identified by the naked eye in three distinct modes. Evidence is collected in aspects concerning cell contractility, cellular morphology, protein expression, and transcriptome profile to show that both the M medium and the scaffold are critical for cell maturation, formation of communicating cellular networks, and regeneration of contractile function. More interestingly, in-depth transcriptional analysis reveals that biological factors in the M medium actively modulate channel activities in cells while the scaffold surprisingly regulates cell-cell communication. We perform interactome analysis of ligand-receptor interactions to visualize the scaffold-induced changes in intercellular communication and discover that scaffold-induced strengthened interactions are centered on enteric neurons. Finally, the living intestinal muscle patch undergoes three ‘digesta manipulation’ tasks which recapitulate critical events that often appear in food digestion and absorption. Thus, we provide a living building block, the contracting intestinal muscle patch, for the future engineering of a fully functional intestine.

2. Results and Discussion

2.1. Soft Elastic Matrix to Better Accommodate IMC Contractile Function

Inspired by the natural organization of the intestinal circular and longitudinal smooth muscle layers, we sought to fabricate a scaffold with aligned fibers and an orthogonal-bilayer structure by sequential electrospinning (Figure 1a-b). Previously, similar electrospun scaffolds have been made using PCL.[53] We noted that although highly aligned PCL fibers successfully promoted cellular alignment, combining the PCL scaffold with the M medium only led to creation of intestinal muscle patches with confined, low-amplitude contractions, [53] presumably due to the tough, plastic nature of PCL. As PCL experiences the contractile forces generated by the muscle cells, it undergoes deformation that dissipates the force. We reasoned that a softer scaffold that can elastically deform and recover in response to the force generated by the contracting muscle might be able to better accommodate the muscle function. In this work, we selected gelatin as the material for scaffold fabrication. The gelatin scaffold was further crosslinked by glutaraldehyde to improve the water-resistant ability and thermostability. Gelatin fiber sheets were cut into small rectangles with an area of 0.35 ± 0.09 cm^2 (mean ± S.D., n = 5 scaffolds). Upon water immersion, the scaffold quickly swells, leading to a ~2.9-fold increase in surface area. During the tensile test, the swollen gelatin scaffold exhibited the typical rubber-like stress-strain behavior (n = 7 scaffolds). It fractured at a strain of 39.1 ± 6.8 % (mean ± S.D., n = 7 scaffolds) without exhibiting yield. We achieved the tensile modulus of the wet gelatin scaffold at 0.9 ± 0.2 MPa (mean ± S.D., n = 7 scaffolds, about 38-fold smaller than that of the PCL-based scaffold fabricated in the same way, Figure 1c), closely resembling that of native intestinal tissue.[54,55]

2.2. Diverse Contraction Modes Generated by the Living Intestinal Muscle Patch

Mouse IMCs were seeded on the bilayer gelatin scaffold at a density of 1.25 million cells/cm^2. IMCs on the scaffold were first cultured in the conventional serum-containing P medium for six days to promote cell proliferation. By day 6, IMCs confluently covered the whole scaffold to form an intestinal smooth muscle patch, and the medium was changed to the M medium to promote cell maturation and function. Phalloidin staining of cells on the scaffold revealed that cells were oriented in two mutually perpendicular directions (Figure 2a). Strikingly, only after four days in the M medium did the intestinal muscle patch display coordinated contractions (Video S1-3, Figure 2b-c) that can be easily identified by the naked eye. Such macroscopic contractions differ from previously observed restricted contractions in cells cultured on a well plate or a PCL scaffold.[53] In response to the contractile forces generated by IMCs, the whole scaffold exhibited dramatic large-scale mechanical deformation and recovery in repeated cycles (Video S1-3, Figure 2b-c). Even more surprisingly, three different contraction modes with distinct fluidic flow-generating behaviors were observed (Figure 2b-c). A dominant contraction mode (22 out of 27 biologically independent samples), the ‘clamshell’ mode, caused the entire intestinal muscle patch to roll up and undergo a clamshell-like opening and closing along a fixed bending axis, reminiscent of the segmental ring motions of the intestinal wall (Figure 2b, Video S1). In some cases, the coordinated contractions of IMCs can significantly curl up the whole muscle patch into a tight scroll structure (Video S1, Sample 1). In another contraction mode (2 out of 27 samples), the ‘jellyfish’ mode, instead of contracting along a fixed axis, IMCs demonstrated a coordinated squeeze-type contraction so that the entire muscle patch curled up into an umbrella shape (Figure 2b, Video S3). As IMCs contracted, the size of the umbrella shrank, and the height of the umbrella grew (Figure 2b, Video S3). The jellyfish mode may correspond to a type of contraction that creates a pouch-like space to constrict around the food chyme and gradually scrunch it during digestion. For the third contraction mode (3 out of 27 samples), the ‘oceanwave’ mode, IMCs exhibited ‘peristalsis-like’ contractions that propagated within the muscle patch (Figure 2b, Video S2). The contraction waves wrinkled the muscle patch at several different sites (Figure 2b, Video S2). Those spontaneous macroscopic contractions occurred at an average frequency of 20 contractions per minute (0.33 Hz, Figure 2c) and persisted for at least a month in vitro. Two things concerning the display of macroscopic contractions by the intestinal muscle patch are worth mentioning. First, we note that IMCs seeded on the gelatin scaffold did not show any distinct movement when cultured in the P medium (−M medium, + gelatin scaffold). In the meanwhile, without the presence of the gelatin scaffold but to culture IMCs in the M medium in 2D only created local contracting clusters (+M medium, −gelatin scaffold). Neither of the conditions supports the generation of macroscopic contractions seen here when IMCs were cultured on the gelatin scaffold in the M medium (+M medium, + gelatin scaffold). These results, in combination, demonstrate that such unprecedented strong, diverse contractile motions of the intestinal muscle patch are achieved under an integrated influence of both the M medium and the gelatin scaffold. Second, both the aligned fiber structure and the orthogonal bi-layered organization mimic the natural architecture of the intestinal muscle tissue. Such structural features actively guide cell organization (as seen in previous literature[41,53,56] and the next section of this article) and may facilitate better cell communication for quick mechano-transduction. However, in addition to rebuilding

such structural features, selecting a soft elastic material (such as gelatin), but not a tough plastic material (such as PCL), for scaffold fabrication is more critical to the generation of macroscopic muscle contraction, as cells cultured on a PCL-based electrospun scaffold with orientated fibers in the M medium only demonstrate rigid small-scale contractions.[53]

2.3. Enhanced Phenotypic Maturation of Cells in the Intestinal Muscle Patch

Gut motility results from the cooperating work of SMCs, ICCs, and the ENS. In the 2D culture using the M medium (hereafter referred to as the 'M medium' condition), we were able to preserve those cells' function for a prolonged period in vitro.[53] We created the intestinal muscle patch by combining the use of the gelatin scaffold and the use of the M medium (the 'M medium + S' condition; S, scaffold). Under this 'M medium + S' condition, SMCs, ICCs, neurons, and glial cells were partially aligned by the oriented gelatin fibers (Figure 3a). We detected a marked increase in the expression of the SMC marker MHC (myosin heavy chain), the ICC marker c-Kit, the neuronal marker β-tubulin III, and the glial marker GFAP in the 'M medium + S' condition as compared to that in the 'M medium' condition without a scaffold (Figure 3, immunostaining, n = 3 biologically independent samples; RT-PCR, n = 5 biologically independent samples). Unlike the scattered c-Kit$^+$ cell clusters formed in the 'M medium' condition, a dense network of c-Kit$^+$ ICCs expanded throughout the entire intestinal muscle patch in the 'M medium + S' condition (Figure 3a). The 'M medium + S' condition also resulted in the generation of a denser 'ganglionated' neural plexus of β-tubulin III$^+$ neurons and GFAP$^+$ glia with longer axon extension compared with that in the 'M medium' condition (Figure 3a).

We next examined the transcriptional differences between IMCs cultured in the 'P medium', 'M medium', and 'M medium + S' conditions at the day 28-time point using RNA sequencing. Freshly isolated muscle strips served as a positive control. Principal component analysis (PCA) was performed for a whole-transcriptome comparison among different conditions (Figure 4a). PC1 (62%) and PC2 (27%) grouped the samples by their types. The plot suggested that (*i*) both the soluble biological factors in the M medium and the application of the scaffold can enhance the phenotypic maturation of cells to cause transcriptome shifts toward the native tissue and (*ii*) the intestinal muscle patch growing in the 'M medium + S' condition had a global gene expression profile that most closely resembled that of muscle strips over other conditions (Figure 4a). The same conclusion can also be derived from measurements of Spearman's correlation comparing the four conditions (Figure S1). Based on functional enrichment analysis of the PC loadings, both PC1 and PC2 separated the samples encompassing the biological process "multicellular organismal process" (Table S1). Other biological processes (Table S1) that were highly enriched in PC1 gene loadings were terms involving "regulation of transport" (positive), "synaptic signaling" (positive), and "immune system process" (negative).

Differential gene expression analysis revealed that 3,165 out of 18,415 genes were significantly differentially regulated between the 'M medium' and the 'P medium' conditions (adjusted $P < 0.05$, Benjamini-Hochberg Method, Table S2), and 2,820 out of 18,704 genes were significantly differentially expressed between the 'M medium + S' and 'M medium' conditions (adjusted $P < 0.05$, Benjamini-Hochberg Method, Table S3). Here

we focused on the transcriptional changes in cell lineages involved in the generation of GI motility. We specifically looked at genes related to SMCs, ICCs, and ENS (Figure 4b). Interestingly, 477 genes that were significantly upregulated in the 'M medium' condition compared with the 'P medium' condition (adjusted $P < 0.05$, Benjamini-Hochberg Method) were further significantly induced by the application of the scaffold (adjusted $P < 0.05$, Benjamini-Hochberg Method, 'M medium + S' vs. 'M medium') (Table S2-3). Many of such kind genes were associated with SMCs, ICCs, and ENS, including (*i*) genes involved in the muscle excitation-contraction coupling such as *Mylk*, *Abcc9*, *Kcnf1*, and *Jph2*; (*ii*) *Ano1*, the most specific marker for ICCs;[58] (*iii*) neural marker genes such as *Elavl3*, *Elavl4*; (i*v*) enteric glia markers *S100β* and *Plp1*; (*v*) neuronal subtype-specific genes such as *Nos1*and *Vip* for inhibitory motor neurons, *Calb2* and *Tac1* for excitatory motor neurons, and *Gal* for non-cholinergic secretomotor or vasodilator neurons;[59] and (*vi*) genes related to enteric neuronal development such as *Ret*, *Phox2b*, *Gfra1*, *Sox10,* and *Ascl1* (Figure 4b).

Comparing the 'M medium' condition with the 'P medium' condition, a gene ontology (GO) analysis for upregulated genes (adjusted $P > 0.05$, Benjamini-Hochberg Method, log2FoldChange > 0) highlighted a significant enrichment in GO-BP (biological process) terms related to nervous system development and neuron differentiation (Table S4). Correspondingly, GO-CC (cellular component) analysis of differentially expressed genes (adjusted $P > 0.05$, Benjamini-Hochberg Method) revealed significant differences relating to neuron part and synapse between IMCs in the 'M medium' and the 'P medium' condition (Figure 4c, Table S5). Interestingly, the top 10 significant GO-MF (molecular function) terms were primarily related to ion channel activity (Figure 4c, Table S6), indicating the extensive changes in channel activity induced by biological factors in the M medium. In addition, the GO terms "smooth muscle contraction" (FDR = 2.24e-05), "muscle system process" (FDR = 1.56e-18), and "muscle tissue development" (FDR = 2.19e-10) were also significantly enriched for differentially expressed genes.

To investigate the cellular processes where the scaffold may have a regulatory role, we performed the GO analysis for the differentially expressed genes (adjusted $P > 0.05$, Benjamini-Hochberg Method) comparing the intestinal muscle patch versus its 2D counterpart ('M medium + S' vs. 'M medium', Figure 4c, Table S7-9). We found that those genes were highly enriched in biological processes implicated in cell communication, nervous system development, and cell adhesion (Figure 4c, Table S7). For the GO-CC analysis, the intestinal muscle patch profile showed strong enrichment concerning neuron part, synapse, cell junction, and plasma membrane region (Figure 4c, Table S8). In examining the GO-MF (molecular function) terms, 6 out of the top 10 enriched terms are about protein binding, which is the primary way cells communicate with each other and with the environment (Figure 4c, Table S9). Intestinal muscle patch also demonstrated enrichment in GO terms relating to smooth muscle development and function, such as "smooth muscle contraction" (FDR = 3.75e-09), "muscle system process" (FDR = 7.06e-16), and "muscle tissue development" (FDR = 4.24e-10).

All the results suggest that both the M medium and the scaffold promote the maturation of the various cell types that enable GI motility. The relatively high degree of similarities in transcriptome between the intestinal muscle patch and the muscle strips is achieved

by a combined effect of the M medium and the scaffold. In cooperation, the M medium and the scaffold greatly enhance the differentiation and maturity of the ENS, as shown by immunostaining of neuronal and glial markers in different conditions (Figure 3) and the highly enriched ENS-related GO terms for upregulated genes in the 'M medium' condition relative to the 'P medium' condition and those in the 'M medium + S' condition relative to the 'M medium' condition (Table S4, S7). Separately, the M medium profoundly impacts ion transport activities (Figure 4c, GO-MF analysis). The scaffold markedly reshapes cell communication and protein binding (Figure 4c, GO-BP and GO-MF analyses).

2.4. The Intercellular Communication Transformed by the Gelatin Scaffold

Gut motility relies on the highly coordinated functioning of various cells. Such coordination of cellular activities is governed by communication across multiple cell types.[14] Cell-cell communication also plays an essential role in cell differentiation and tissue development.[60] According to our GO analysis, the gelatin scaffold possesses a strong ability to regulate cell-cell communication and receptor binding events that happen within the cells growing on it (Figure 4c, Table S7, S9, highly enriched GO-BP term "regulation of cell communication" and GO-MF terms related to protein binding). Cell-cell signaling extensively depends on and can be inferred by ligand-receptor interactions.[60,61] We further interrogated how the scaffold-driven changes in gene expression might influence cell-cell communication within the intestinal muscle patch by studying the interacting ligand-receptor pairs. Among 2,820 differentially expressed genes in the intestinal muscle patch compared to its 2D counterpart (adjusted $P < 0.05$, Benjamini-Hochberg Method, 'M medium + S' condition vs. 'M medium' condition), 693 genes (25%) encode receptor, ligand, or ECM (extracellular matrix) proteins (Figure 5a, see ref. [61] for the definition of receptors, ligands, and ECM proteins). Based on a published cell communication interactome,[61] we extracted the ligand-receptor interactions that were mostly affected by the presence of the gelatin scaffold (adjusted $P < 0.001$, Benjamini-Hochberg Method, |Log2FoldChange| >1, Figure 5b-c, Table S10-11). We only considered the scenarios when the ligand and the paired receptor genes were both scaffold-upregulated (70 pairs, gain of interaction) or both scaffold-downregulated (53 pairs, loss of interaction). Among the 70 upregulated ligand-receptor pairs, 55 pairs (78%) were involved in ENS development and function (Figure 5b, Table S10), indicating that the potentially strengthened interactions were centered on the enteric neurons. The gene encoding the tyrosine kinase receptor, *RET*, is most commonly mutated in Hirschsprung's disease.[62] The RET/GFRα1/GDNF pathway is perhaps the most important pathway in ENS development.[62] Loss of *Ret*, *Gdnf*, or *Gfra1* leads to complete intestinal aganglionosis in mice.[62] In the intestinal muscle patch, compared with its 2D counterpart, both *Ret* – *Gdnf* and *Gdnf* – *Gfra1* were among the highly upregulated interacting pairs (Figure 5b, Table S10). Another two RET-specific ligand genes *Artn* (Figure 5b, Table S10) and *Nrtn* (adjusted $P = 0.005$, Log2FoldChange = 0.83) also showed significantly increased expression in the intestinal muscle patch. Other important ENS-related interactions induced by the scaffold include *Ednra* – *Edn3*, *Npy* – *Npy4r*, *Ngfr* – *Ntf3*, *Ntrk1* – *Ntf3*, and *Sorcs2* – *Ntf3* (Figure 5b, Table S10). Previous studies have shown that ICCs and SMCs express manifold neurotransmitter receptors, including the tachykinin receptor (encoded by *Tacr1*), an excitatory neurotransmitter receptor, and the vasoactive intestinal peptide receptor 2 (encoded by *Vipr2*), the receptor of the

inhibitory neurotransmitter VIP.[63,64] In the intestinal muscle patch, the ligand-receptor pairs *Tac1* – *Tacr1* and *Vip* – *Vipr2* (adjusted $P = 0.002$) were significantly upregulated, indicating a potentially enhanced information transfer between enteric neurons and/or from enteric neurons to ICCs or SMCs (Figure 5b, Table S10). Among the potentially boosted communication pairs that were not ENS-related, some were putatively involved in smooth muscle development (*Itga7*[65] – collagen genes, Figure 5b, Table S10). The rest were associated with tissue development, extracellular matrix organization, and immune system process (Figure 5b, Table S10). For the decreased interactions, the affected ligand-receptor pairs were primarily related to cell migration and cell motility (Figure 5c, Table S11), suggesting that the contact guidance exerted by the scaffold may restrict certain motility events that are commonly seen in 2D cultures.

2.5. Macroscopic Contractions to Mix and Breakdown Artificial Intestinal Contents

GI muscle contraction promotes the physical breakdown of the ingested meal to facilitate efficient food digestion. To evaluate the functional performance of the intestinal muscle patch in mixing and handling the intestinal contents, we challenged the intestinal muscle patch with three “digesta manipulation” tasks: (*i*) enhance the local mixing of liquid; (*ii*) triturate large pieces of viscous artificial digesta; and (*iii*) accelerate the solubilization process to facilitate better absorption (Figure 6, Video S4-6). The intestinal muscle patch can generate three different contraction modes: the ‘clamshell’, ‘jellyfish’, and ‘oceanwave’ (Figure 2, Video S1-3). We believe that each mode produces its own unique mechanical force pattern that may have different effects when handling the digesta. Due to the limited number of intestinal muscle patches showing the ‘jellyfish’ and ‘oceanwave’ contractions, in this part, we only tested the intestinal muscle patches in the ‘clamshell’ contraction mode. A cell-free scaffold served as the negative control. All the experiments were conducted at the physiological temperature (37 °C).

In the first task, four μl of colored culture medium was dropped on top of the contracting intestinal muscle patch or the control scaffold (Figure 6a, Video S4). Contractions of the intestinal muscle patch quickly mixed the blue-colored medium with the surrounding liquid in less than 30 seconds, a process much faster than the mix via diffusion as seen in the control condition (Figure 6a, Video S4, n = 3 biologically independent samples). In the second task, we created a flour-based artificial digest that matched the viscoelastic properties of the real food chyme found in the proximal small intestine (Figure 6b, Video S5).[66,67] The digesta obtained from the animal intestine is characteristic of a weak shear-thinning viscoelastic gel.[66,67] Such features were successfully captured by the artificial digesta, as indicated by the dynamic rheological measurements (Figure 6b). We were particularly interested in the viscoelastic behavior of the artificial digesta at the oscillation frequency close to the average contraction rate of the intestinal muscle patch, i.e., 0.33 Hz (20 contractions per minute, Figure 2c). At 0.33 Hz, a strain sweep (0.6% −100%) showed that, as expected for a weak gel, within the linear viscoelastic regime, the storage (elastic) modulus consistently exceeded the loss (viscous) modulus, however, the storage modulus dropped rapidly as the strain increased and became smaller than the loss modulus (Figure 6b). In a frequency sweep at a constant strain of 5%, we found that (*i*) the storage modulus was consistently higher than the loss modulus throughout the physiological frequency range

(0.04 – 1 Hz, possible muscle contraction rate); (*ii*) the two moduli differed by less than an order of magnitude; and (*iii*) both moduli slightly increased with the oscillation frequency: all indicate the formation of a weak viscoelastic gel (Figure 6b). When applying the artificial digesta to the intestinal muscle patch, a 3-mm-sized artificial digesta drop can be completely broken down by ~ 10 contractions within 30 seconds (Figure 6b, Video S5). Without the contracting intestinal muscle patch, for over 2 minutes, the drop of the artificial digesta, though slightly swelled, kept its shape and remained stable in the culture medium with no apparent mixing with the surrounding liquid phase (Figure 6b, Video S5). In the third task, a non-crosslinked gelatin capsule containing green-colored glycerol was employed, and we found that compared with the control, the contraction of the intestinal muscle patch markedly accelerated the solubilization of the gelatin capsule to enable a much faster release of the encapsulated, green-colored content (Figure 6c, Video S6). Such enhanced solubilization facilitated by the macroscopic contractions may promote a more efficient breakdown and absorption of food macronutrients.

3. Conclusion

In this work, we successfully created a contracting intestinal muscle patch through the synergism between biochemical signals from a culture medium and environmental cues exerted by a scaffold. The contractility of the intestinal muscle patch outperforms the existing engineered intestinal muscle in terms of the diversity of the contraction and the amplitude of the movement. For the first time in vitro, an engineered intestinal muscle displays a record strength of contractility to enable the mixing and physical breakdown of viscoelastic gels that mimic the mechanical properties of the intestinal digesta. The intestinal muscle patch recapitulates the critical cellular components involved in the generation of gut motility and demonstrates a closer transcriptional approximation of the native intestinal muscle. It is well known that a bioscaffold can provide biomechanical support and topological guidance for cell growth and differentiation, but here we unveil a previously overlooked effect of the scaffold to show that a bioscaffold is also capable of regulating intercellular communication. 78% of the scaffold-induced gain of interaction relates to enteric neurons, suggesting that, compared with other types of cells in the culture, such as SMCs and ICCs, neurons are more responsive to the material's stimulation under the current experimental condition. Other materials that can better manipulate SMCs and ICCs may be required in the future design of the scaffold. Future experiments must systematically elucidate how different types of cells can show different responsiveness to the same materials. In addition, interactive pairs in RET/GFRα1/GDNF pathway are highly upregulated by the presence of the scaffold, suggesting that the regeneration of enteric neurons under the influence of the gelatin scaffold utilizes canonical developmental pathways. Proven methods in material design that will enhance the canonical developmental pathways in ENS development may be worth incorporating into the current scaffold for enhanced maturation of enteric neurons.

Although the intestinal muscle patch exhibits unprecedented contractility and achieves what the muscle strips can basically do in vitro, i.e., macroscopic contractions displayed in different contraction modes, we acknowledge that there are differences between the intestinal muscle patch and the muscle strip. By performing PCA between the intestinal

muscle patch and the muscle strips, we identified the major aspects where the two conditions show the most variations at the transcriptome level. We found that they mainly differ in the population of immune cells (Figure S2). Integrating the correct immune cell population into the culture may help reconstruct neuroimmune circuits, which in turn regulates the temporal and spatial control of muscle contraction. The realization of higher-order contraction motion and fine-tuning of muscle contraction may also depend on (*i*) precise reconstruction of the architecture of the networks of ENS, SMCs, and ICCs at single-cell resolution; (*ii*) maximized preservation of every single type of cells in the muscle layer; (*iii*) precise recapitulation of the mechanical structure and properties of intestinal muscle tissue; and (*iv*) functional integration of the muscle layer with the intestinal epithelia layers. The intestinal muscle patch created here sets the basis for reconstructing the full-thickness engineered intestine to treat SBS. The technique established in this work may eventually help bring within reach the current “impossible dream” of engineering a fully functional intestine capable of generating dynamic complex motor patterns in the future.

Supplementary Material

Refer to Web version on PubMed Central for supplementary material.

Acknowledgments

We thank S. Vijayakumar for her technical advice. We thank the UCLA BSCRC High Throughput Sequencing Core. This work was supported by NIH U01 DK085535 and R01DK130972 (to J.C.Y.D. and M.G.M.) and a scholarship from China Scholarship Council (to Q.W.). Part of this work was performed at the Stanford Nano Shared Facilities (SNSF), Soft & Hybrid Materials Facility (SMF), supported by the National Science Foundation under award ECCS-2026822, and at Stanford University Cell Sciences Imaging Core Facility (RRID:SCR_017787). ToC figure of this article is created with BioRender.com.

Data availability Statement

RNA-seq data have been submitted to the NCBI GEO under the accession number GSE223116. Further information and requests for data should be directed to the corresponding authors.

References

[1]. Merritt RJ, Cohran V, Raphael BP, Sentongo T, Volpert D, Warner BW, Goday PS, J Pediatr Gastroenterol Nutr 2017, 65, 588. [PubMed: 28837507]

[2]. Chandra R, Kesavan A, Clin J Gastroenterol 2018, 11, 103. [PubMed: 29280097]

[3]. Massironi S, Cavalcoli F, Rausa E, Invernizzi P, Braga M, Vecchi M, Digestive and Liver Disease 2020, 52, 253. [PubMed: 31892505]

[4]. Pironi L, Corcos O, Forbes A, Holst M, Joly F, Jonkers C, Klek S, Lal S, Blaser AR, Rollins KE, Sasdelli AS, Shaffer J, van Gossum A, Wanten G, Zanfi C, Lobo DN, Clinical Nutrition 2018, 37, 1798. [PubMed: 30172658]

[5]. Goulet O, Nader EA, Pigneur B, Lambe C, Pediatr Gastroenterol Hepatol Nutr 2019, 22, 303. [PubMed: 31338307]

[6]. Tullie L, Jones BC, de Coppi P, Li VSW, Nat Rev Gastroenterol Hepatol 2022, DOI 10.1038/s41575-022-00586-x.

[7]. Mutanen A, Wales PW, Semin Pediatr Surg 2018, 27, 209. [PubMed: 30342594]

[8]. Kurpios NA, Ibañes M, Davis NM, Lui W, Katz T, Martin JF, Belmonte JCI, Tabin CJ, Proc Natl Acad Sci U S A 2008, 105, 8499. [PubMed: 18574143]

[9]. Savin T, Kurpios NA, Shyer AE, Florescu P, Liang H, Mahadevan L, Tabin CJ, Nature 2011, 476, 57. [PubMed: 21814276]

[10]. Shyer AE, Huycke TR, Lee C, Mahadevan L, Tabin CJ, Cell 2015, 161, 569. [PubMed: 25865482]

[11]. Shyer AE, Tallinen T, Nerurkar NL, Wei Z, Gil ES, Kaplan DL, Tabin CJ, Mahadevan L, Science (1979) 2013, 342, 212.

[12]. Holloway EM, Czerwinski M, Tsai YH, Wu JH, Wu A, Childs CJ, Walton KD, Sweet CW, Yu Q, Glass I, Treutlein B, Camp JG, Spence JR, Cell Stem Cell 2021, 28, 568. [PubMed: 33278341]

[13]. Martín-Alonso M, Iqbal S, Vornewald PM, Lindholm HT, Damen MJ, Martínez F, Hoel S, Díez-Sánchez A, Altelaar M, Katajisto P, Arroyo AG, Oudhoff MJ, Nat Commun 2021, 12, DOI 10.1038/s41467-021-26904-6.

[14]. Sanders KM, Koh SD, Ro S, Ward SM, Nat Rev Gastroenterol Hepatol 2012, 9, 633. [PubMed: 22965426]

[15]. Koppen IJN, Benninga MA, Singendonk MMJ, Early Hum Dev 2017, 114, 1. [PubMed: 28927754]

[16]. Deloose E, Janssen P, Depoortere I, Tack J, Nat Rev Gastroenterol Hepatol 2012, 9, 271. [PubMed: 22450306]

[17]. Sanders KM, Eur Rev Med Pharmacol Sci 2008, 12, 129. [PubMed: 18924452]

[18]. Torihashi S, Ward SM, Nishikawa SI, Nishi K, Kobayashi S, Sanders KM, Cell Tissue Res 1995, 280, DOI 10.1007/BF00304515.

[19]. Hulzinga JD, Thuneberg L, Klüppel M, Malysz J, Mikkelsen HB, Bernstein A, Nature 1995, 373, DOI 10.1038/373347a0.

[20]. Ward SM, Burns AJ, Torihashi S, Sanders KM, Mutation of the Proto-Oncogene c-Kit Blocks Development of Interstitial Cells and Electrical Rhythmicity in Murine Intestine, 1994.

[21]. Bayliss WM, Starling EH, J Physiol 1899, 24, DOI 10.1113/jphysiol.1899.sp000752.

[22]. Kosterlitz HW, Pirie VW, Robinson JA, J Physiol 1956, 133, DOI 10.1113/jphysiol.1956.sp005618.

[23]. Hirst GD, Holman ME, McKirdy HC, J Physiol 1975, 244, DOI 10.1113/jphysiol.1975.sp010786.

[24]. Spencer N, Walsh M, Smith TK, Journal of Physiology 1999, 517, 889. [PubMed: 10358127]

[25]. Furness JB, Nat Rev Gastroenterol Hepatol 2012, 9, 286. [PubMed: 22392290]

[26]. Mercado-Perez A, Beyder A, Nat Rev Gastroenterol Hepatol 2022, DOI 10.1038/s41575-021-00561-y.

[27]. Kim M, Heo G, Kim SY, Nat Rev Neurosci 2022, 23, 135. [PubMed: 34983992]

[28]. Spencer NJ, Hu H, Nat Rev Gastroenterol Hepatol 2020, 17, 338. [PubMed: 32152479]

[29]. Rao M, Nat Rev Gastroenterol Hepatol 2020, 17, 72. [PubMed: 31811278]

[30]. Huh JR, Veiga-Fernandes H, Nat Rev Immunol 2020, 20, 217. [PubMed: 31848462]

[31]. Fattahi F, Steinbeck JA, Kriks S, Tchieu J, Zimmer B, Kishinevsky S, Zeltner N, Mica Y, El-Nachef W, Zhao H, de Stanchina E, Gershon MD, Grikscheit TC, Chen S, Studer L, Nature 2016, 531, 105. [PubMed: 26863197]

[32]. Dickman CTD, Russo V, Thain K, Pan S, Beyer ST, Walus K, Getsios S, Mohamed T, Wadsworth SJ, FASEB Journal 2020, 34, 1652. [PubMed: 31914670]

[33]. Dadhich P, Bitar KN, Stem Cells Transl Med 2020, 9, 713. [PubMed: 32181603]

[34]. Tamama K, Sen CK, Wells A, Stem Cells Dev 2008, 17, 897. [PubMed: 18564029]

[35]. Ghionzoli M, Repele A, Sartiani L, Costanzi G, Parenti A, Spinelli V, David AL, Garriboli M, Totonelli G, Tian J, Andreadis ST, Cerbai E, Mugelli A, Messineo A, Pierro A, Eaton S, de Coppi P, FASEB Journal 2013, 27, 4853. [PubMed: 23995291]

[36]. Ootani A, Li X, Sangiorgi E, Ho QT, Ueno H, Toda S, Sugihara H, Fujimoto K, Weissman IL, Capecchi MR, Kuo CJ, Nat Med 2009, 15, 701. [PubMed: 19398967]

[37]. Dimarco RL, Su J, Yan KS, Dewi R, Kuo CJ, Heilshorn SC, Integrative Biology (United Kingdom) 2014, 6, 127.

[38]. Nakayama S, Torihashi S, Japanese Journal of Physiology 2002, 52, 217. [PubMed: 12139780]

[39]. Espinosa-Luna R, Barajas-Espinosa AR, Ochoa-Cortez F, Barajas-López C, in Methods in Molecular Biology, 2018.

[40]. Walthers CM, Lee M, Wu BM, Dunn JCY, PLoS One 2014, 9, e114850. [PubMed: 25486279]

[41]. Kobayashi M, Khalil HA, Lei NY, Wang Q, Wang K, Wu BM, Dunn JCY, Sci Rep 2018, 8, 13544. [PubMed: 30202095]

[42]. Kuwahara M, Ogaeri T, Matsuura R, Kogo H, Fujimoto T, Torihashi S, Neurogastroenterology and Motility 2004, 16, 14. [PubMed: 15065998]

[43]. Yamada T, Yoshikawa M, Takaki M, Torihashi S, Kato Y, Nakajima Y, Ishizaka S, Tsunoda Y, Stem Cells 2002, 20, 41. [PubMed: 11796921]

[44]. Ito-Dufros Y, Funakoshi Y, Uehara A, Oishi K, Neurogastroenterology and Motility 2007, 19, 288. [PubMed: 17391245]

[45]. Yoshida A, Chitcholtan K, Evans JJ, Nock V, Beasley SW, J Pediatr Surg 2012, 47, 329. [PubMed: 22325385]

[46]. Watson CL, Mahe MM, Múnera J, Howell JC, Sundaram N, Poling HM, Schweitzer JI, Vallance JE, Mayhew CN, Sun Y, Grabowski G, Finkbeiner SR, Spence JR, Shroyer NF, Wells JM, Helmrath MA, Nat Med 2014, 20, DOI 10.1038/nm.3737.

[47]. McCracken KW, Howell JC, Wells JM, Spence JR, Nat Protoc 2011, 6, DOI 10.1038/nprot.2011.410.

[48]. Spence JR, Mayhew CN, Rankin SA, Kuhar MF, Vallance JE, Tolle K, Hoskins EE, Kalinichenko V. v., Wells SI, Zorn AM, Shroyer NF, Wells JM, Nature 2011, 470, DOI 10.1038/nature09691.

[49]. Workman MJ, Mahe MM, Trisno S, Poling HM, Watson CL, Sundaram N, Chang CF, Schiesser J, Aubert P, Stanley EG, Elefanty AG, Miyaoka Y, Mandegar MA, Conklin BR, Neunlist M, Brugmann SA, Helmrath MA, Wells JM, Nat Med 2017, 23, 49. [PubMed: 27869805]

[50]. Schlieve CR, Fowler KL, Thornton M, Huang S, Hajjali I, Hou X, Grubbs B, Spence JR, Grikscheit TC, Stem Cell Reports 2017, 9, 883. [PubMed: 28803915]

[51]. Yuan H, Hu H, Chen R, Mu W, Wang L, Li Y, Chen Y, Ding X, Xi Y, Mao SS, Jiang M, Chen J, He Y, Wang L, Dong Y, Tou J, Chen W, Stem Cells Transl Med 2021, 10, 922. [PubMed: 33481357]

[52]. Poling HM, Wu D, Brown N, Baker M, Hausfeld TA, Huynh N, Chaffron S, Dunn JCY, Hogan SP, Wells JM, Helmrath MA, Mahe MM, Nat Biomed Eng 2018, 2, 429. [PubMed: 30151330]

[53]. Wang Q, Wang K, Sergio Solorzano-Vargas R, Lin PY, Walthers CM, Thomas AL, Martín MG, Dunn JCY, PLoS One 2018, 13, DOI 10.1371/journal.pone.0195315.

[54]. Hosseini HS, Dunn JCY, Bioengineering 2020, 7, 1.

[55]. Bourgouin S, Bège T, Masson C, Arnoux PJ, Mancini J, Garcia S, Brunet C, Berdah S. v., Med Biol Eng Comput 2012, 50, 1279. [PubMed: 23054381]

[56]. Kobayashi M, Lei NY, Wang Q, Wu BM, Dunn JCY, Biomaterials 2015, 61, 75. [PubMed: 26001072]

[57]. Schneider CA, Rasband WS, Eliceiri KW, Nat Methods 2012, 9, DOI 10.1038/nmeth.2089.

[58]. Gomez-Pinilla PJ, Gibbons SJ, Bardsley MR, Lorincz A, Pozo MJ, Pasricha PJ, van de Rijn M, West RB, Sarr MG, Kendrick ML, Cima RR, Dozois EJ, Larson DW, Ordog T, Farrugia G, Am J Physiol Gastrointest Liver Physiol 2009, 296, DOI 10.1152/ajpgi.00074.2009.

[59]. Furness JB, J Auton Nerv Syst 2000, 81, 87. [PubMed: 10869706]

[60]. Armingol E, Officer A, Harismendy O, Lewis NE, Nat Rev Genet 2021, 22, DOI 10.1038/s41576-020-00292-x.

[61]. Ximerakis M, Lipnick SL, Innes BT, Simmons SK, Adiconis X, Dionne D, Mayweather BA, Nguyen L, Niziolek Z, Ozek C, Butty VL, Isserlin R, Buchanan SM, Levine SS, Regev A, Bader GD, Levin JZ, Rubin LL, Nat Neurosci 2019, 22, DOI 10.1038/s41593-019-0491-3.

[62]. Lake JI, Heuckeroth RO, Am J Physiol Gastrointest Liver Physiol 2013, 305, DOI 10.1152/ajpgi.00452.2012.

[63]. Chen H, Ördög T, Chen J, Young DL, Bardsley MR, Redelman D, Ward SM, Sanders KM, Physiol Genomics 2007, 31, DOI 10.1152/physiolgenomics.00113.2007.

[64]. Chen H, Redelman D, Ro S, Ward SM, Ördög T, Sanders KM, Am J Physiol Cell Physiol 2007, 292, DOI 10.1152/ajpcell.00147.2006.

[65]. Guo C, Willem M, Werner A, Raivich G, Emerson M, Neyses L, Mayer U, Hum Mol Genet 2006, 15, DOI 10.1093/hmg/ddl018.

[66]. Lentle RG, Janssen PWM, J Comp Physiol B 2008, 178, DOI 10.1007/s00360-008-0264-x.

[67]. Lentle RG, Hemar Y, Hall CE, Stafford KJ, J Comp Physiol B 2005, 175, DOI 10.1007/s00360-005-0490-4.

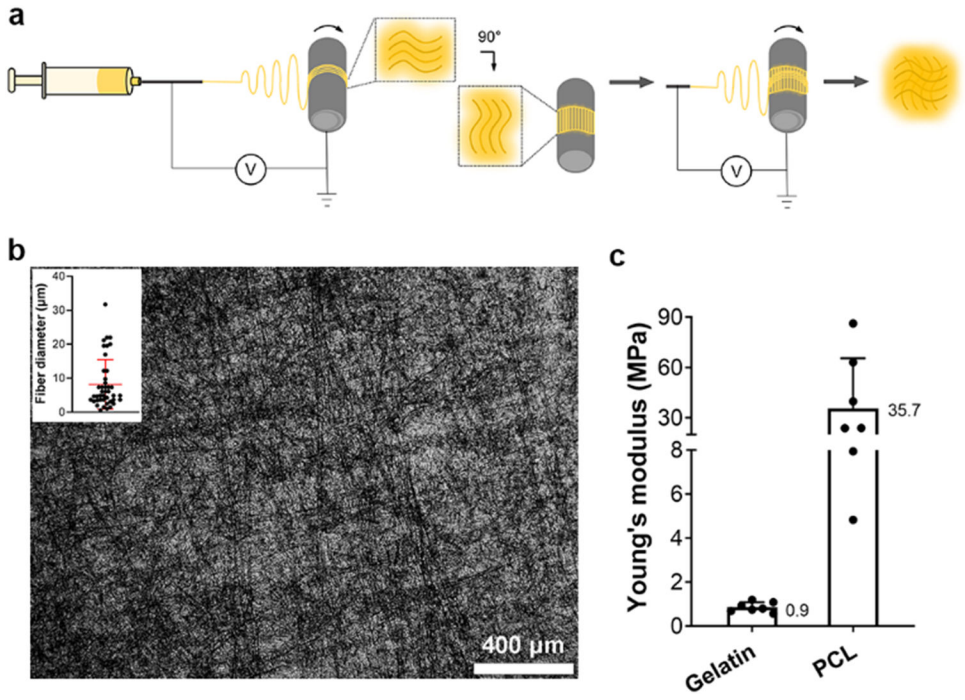

Figure 1.

Fabrication and characterization of the gelatin scaffold. a) Schematic for fabrication of the 0°-90° bilayer electrospun gelatin scaffold. b) Light microscopic image of the wet gelatin scaffold (n = 3 samples) with an inset to show the measurements of the fiber diameter (n = 3 scaffolds). Fibers were orthogonally aligned. c) Young's modulus of bilayer scaffolds made of gelatin or PCL (mean ± s.d., n = 7 samples).

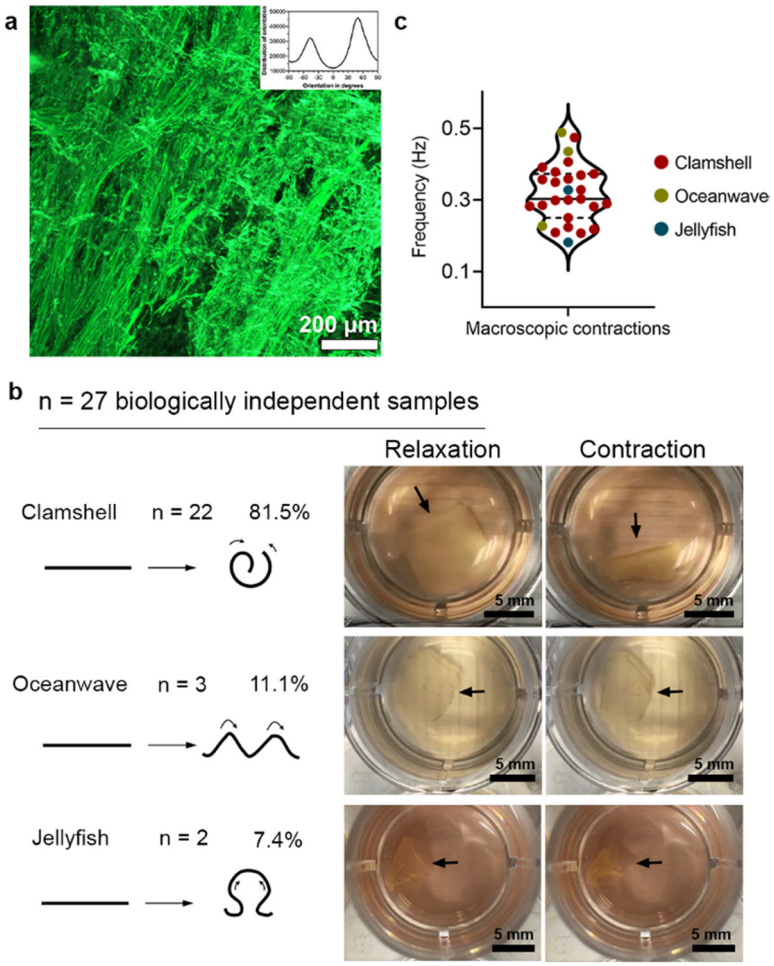

Figure 2.

Diverse contraction modes generated by the living intestinal muscle patch. a) Phalloidin staining of IMCs on the gelatin scaffold at day 28 in the M medium (n = 3 biologically independent samples) with inset to show the measurement of cell orientation (ImageJ[57]). b) Three different contraction modes: clamshell, oceanwave, and jellyfish. Left, schematic of contractile motions. Right, snapshots of contracting muscle patches at their maximal contraction and relaxation state, corresponding to Video S1, Sample 2 (clamshell, d21 in culture), Video S2 (oceanwave, d28 in culture), and Video S3 (Jellyfish, d35 in culture). Note: although we have shown the three contraction modes at different days of culture in this figure, we would like to point out that contraction modes are not determined or affected by the length of culture. c) Frequency of the macroscopic contractions generated by the living intestinal muscle patches, violin plot showing the median (solid line) and quartiles (dashed line), n = 27 biologically independent samples.

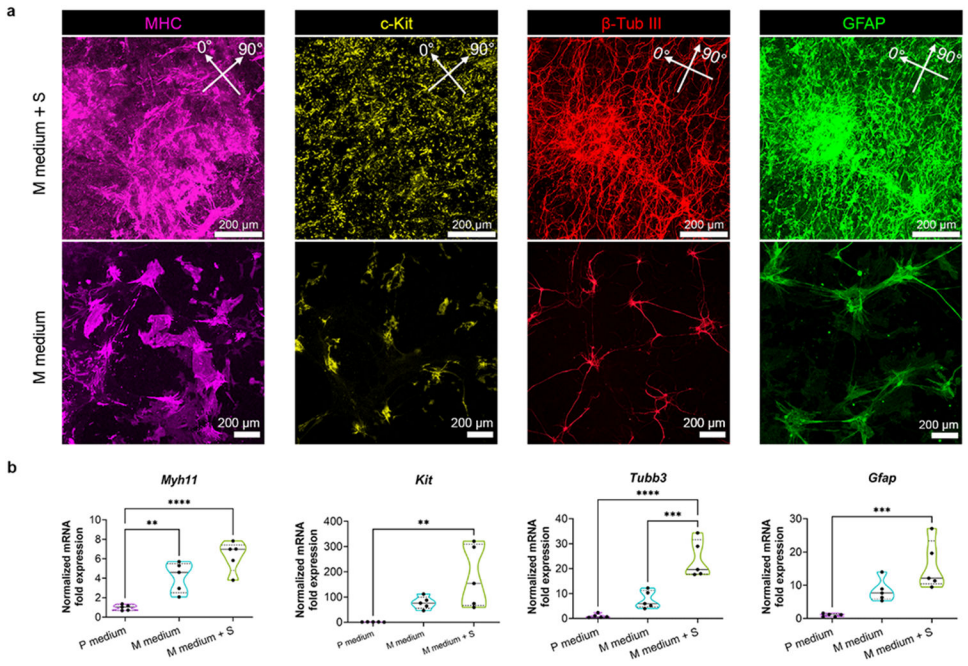

Figure 3.

Enhanced maturation of SMCs, ICCs, and enteric nerves in the intestinal muscle patch. a) Immunofluoresecene analysis of indicated markers in the intestinal muscle patch (the 'M medium + S' condition, d28 in culture, confocal microscope Z-stack images) or IMCs cultured in the M medium on a well-plate (d28 in culture, light microscope images). Arrow sets indicate the gelatin fiber orientations within the scaffold. b) Relative mRNA expression levels of markers for SMCs (*Myh11*), ICC (*Kit*), enteric neurons (*Tubb3*), and enteric glia (*Gfap*) at day 28 in culture. The average expression level of each gene in the 'P medium' was set to 1. *Gapdh* served as the housekeeping gene. Truncated violin plot showing the median (solid line) and quartiles (dashed line). n = 5 biologically independent samples. Statistical analysis for each gene (datasets normally distributed) used one-way analysis of variance (ANOVA) with Tukey's test, **, $p < 0.01$; ***, $p < 0.001$; ****, $p < 0.0001$.

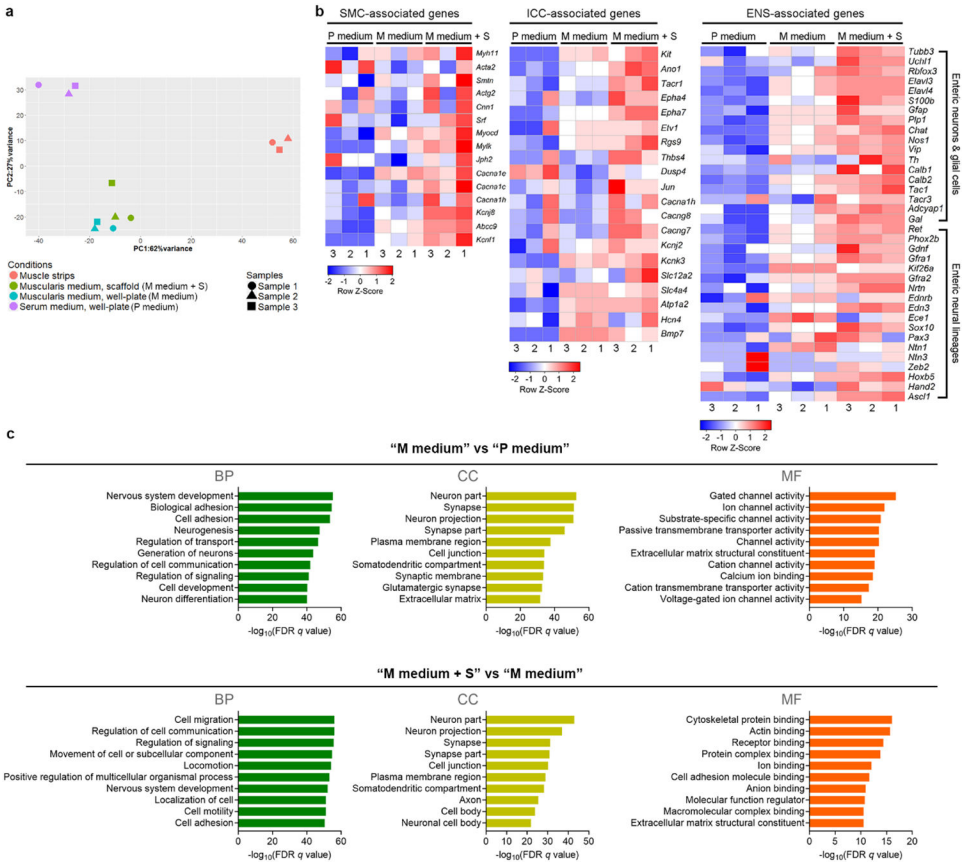

Figure 4.

A transcriptional shift toward the native tissue under the synergistic effect of the 'M medium' and the scaffold. a) PCA of muscle strips, the intestinal muscle patch ('M medium + S' condition), IMCs cultured in 2D in the M medium ('M medium' condition) and in the P medium ('P medium' condition), n = 3 biologically independent samples per condition. Cells were cultured *in vitro* in different conditions for 28 days. b) Heatmaps of RNA-sequencing data for selected SMC, ICC, and ENS-related genes expressed in the 'P medium', 'M medium', and 'M medium + S' conditions, n = 3 biologically independent samples per condition. c) Top 10 GO terms showing differences in gene expression between the 'M medium' and the 'P medium' conditions and between the 'M medium + S' and the 'M medium' conditions. Differentially expressed genes with adjusted $P < 0.05$ (Benjamini-Hochberg Method) were used. BP, biological process; CC, cellular component; MF, molecular function.

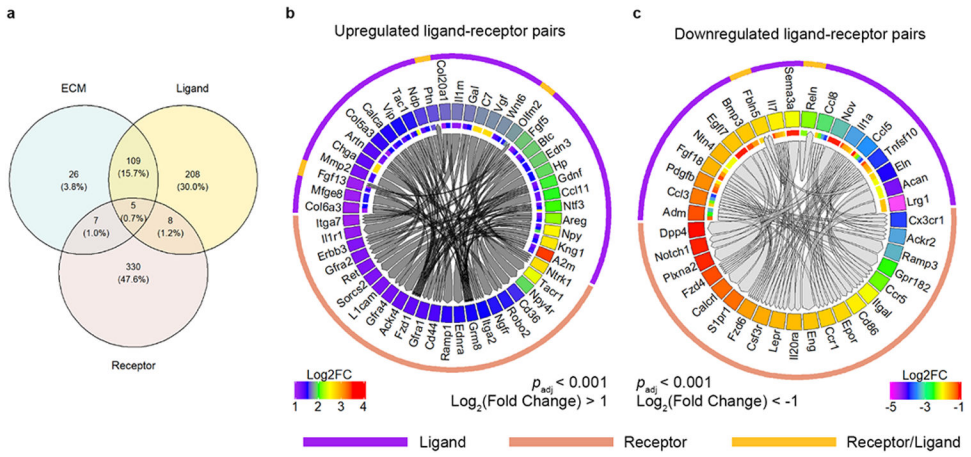

Figure 5.

Scaffold-induced changes in ligand-receptor communication. a) Venn diagram of the number of the ligand, receptor, and ECM genes significantly differentially expressed in the ‘M medium + S’ condition when compared with those in the ‘M medium’ condition (adjusted $P < 0.05$, Benjamini-Hochberg Method). b) and c) Circos plots for most significant alterations in ligand-receptor interactions between the ‘M medium + S’ and the ‘M medium’ conditions (adjusted $P < 0.001$, Benjamini-Hochberg Method), corresponding to Table S10 (ligand and receptor genes both upregulated, panel b) and Table S11 (ligand and receptor genes both downregulated, panel c).

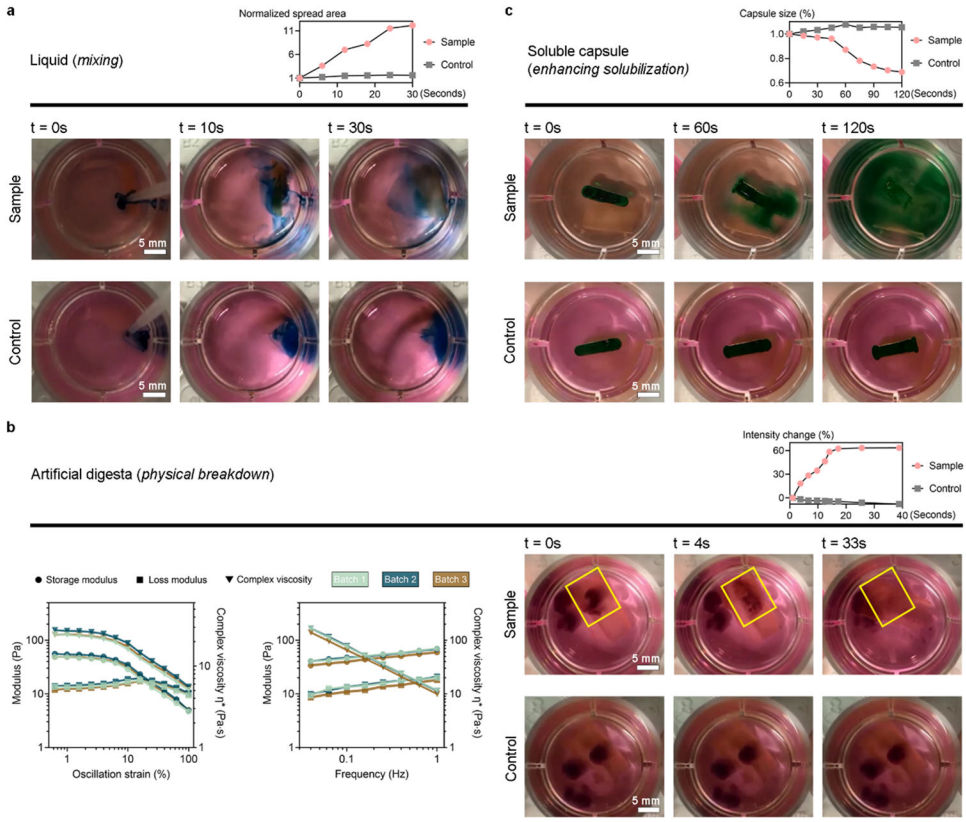

Figure 6.

Three ‘digesta manipulation’ tasks realized by the contracting intestinal muscle patch. a) Enhancing local liquid mixing, corresponding to Video S4. Liquid colored in blue. The liquid mixing process was quantified by measuring the change of the blue-colored area to indicate the spread of the blue-colored medium. The initial size of the blue-colored area at t = 0 was set as 1. b) Physical breakdown of the artificial digesta (purple colored), corresponding to Video S5. Left, rheology of the artificial digesta during strain sweep (0.6% – 100%, at 2.07 rad/s (0.33Hz)) and frequency sweep (0.25 – 6.28 rad/s (0.06 to 1 Hz), at 5% strain). The intensity change of purple-colored digesta was recorded. As the purple-colored artificial digesta was broken into pieces, the purple color also became lighter. c) Accelerating the solubilization process, corresponding to Video S6. Non-crosslinked gelatin capsule was loaded with green-colored glycerol. The size of the capsule was measured to indicate the degree of solubilization of the capsule. The size of the capsule decreased while the capsule was solubilized into the surrounding medium.